Mechanical Systems and Signal Processing 39 (2013) 143–161

Contents lists available at SciVerse ScienceDirect

Mechanical Systems and Signal Processing

journal homepage: www.elsevier.com/locate/ymssp

A functional model based statistical time series method for vibration based damage detection, localization, and magnitude estimation

F.P. Kopsaftopoulos, S.D. Fassois *

Stochastic Mechanical Systems & Automation (SMSA) Laboratory, Department of Mechanical & Aeronautical Engineering, University of Patras, GR 265 00 Patras, Greece

ARTICLE INFO

Article history:
Received 30 November 2010
Received in revised form
24 May 2012
Accepted 30 August 2012
Available online 11 October 2012

Keywords:
Damage detection
Damage identification
Damage quantification
Structural health monitoring
Damage diagnosis
Statistical time series methods

ABSTRACT

A vibration based statistical time series method that is capable of effective damage detection, precise localization, and magnitude estimation within a unified stochastic framework is introduced. The method constitutes an important generalization of the recently introduced functional model based method (FMBM) in that it allows for *precise* damage localization over properly defined *continuous topologies* (instead of pre-defined specific locations) and magnitude estimation for the first time within the context of statistical time series methods that use *partial identified models* and a *limited number of measured signals*. Estimator uncertainties are taken into account, and uncertainty ellipsoids are provided for the damage location and magnitude. The method is based on the extended class of vector-dependent functionally pooled (VFP) models, which are characterized by parameters that depend on both damage magnitude and location, as well as on proper statistical estimation and decision making schemes. The method is validated and its effectiveness is experimentally assessed via a proof-of-concept application to damage detection, precise localization, and magnitude estimation on a prototype GARTEUR-type laboratory scale aircraft skeleton structure. The damage scenarios consist of varying size small masses attached to various continuous topologies on the structure. The method is shown to achieve effective damage detection, precise localization, and magnitude estimation based on even a single pair of measured excitation–response vibration signals.

1. Important conventions and symbols

Definition is indicated by $:=$. Matrix transposition is indicated by the superscript T.
Bold-face upper/lower case symbols designate matrix/column-vector quantities, respectively.

Abbreviation: AR, Autoregressive; ARX, Autoregressive with exogenous excitation; BIC, Bayesian information criterion; FEM, Finite element model; FMBM, Functional model based method; FP, Functionally pooled; FRF, Frequency response function; GA, Genetic algorithm; iid, Identically independently distributed; NLS, Nonlinear least squares; OLS, Ordinary least squares; PE, Prediction error; RSS, Residual sum of squares; SHM, Structural health monitoring; SQP, Sequential quadratic programming; SSS, Signal sum of squares; VFP, Vector-dependent functionally pooled; WLS, Weighted least squares; X, Exogenous.

* Corresponding author. Tel./fax: +30 2610 969 495 (direct); +30 2610 969 492 (central).
E-mail addresses: fkopsaf@mech.upatras.gr (F.P. Kopsaftopoulos), fassois@mech.upatras.gr (S.D. Fassois).
URL: http://www.smsa.upatras.gr (S.D. Fassois).

0888-3270/$ - see front matter © 2012 Elsevier Ltd. All rights reserved.
http://dx.doi.org/10.1016/j.ymssp.2012.08.023

A functional argument in parentheses designates function of a real variable; for instance $P(x)$ is a function of the real variable x.

A functional argument in brackets designates function of an integer variable; for instance $x[t]$ is a function of normalized discrete time ($t=1,2,\ldots$). The conversion from discrete normalized time to analog time is based on $(t-1)T_s$, with T_s designating the sampling period.

A hat designates estimator/estimate; for instance $\widehat{\boldsymbol{\theta}}$ is an estimator/estimate of $\boldsymbol{\theta}$.

2. Introduction

Damage detection, localization, and magnitude estimation (collectively referred to as damage diagnosis, or damage detection and identification) in vibrating structures, including aerospace, mechanical, civil, and marine structures, are of paramount importance for reasons associated with improved dynamic performance, proper operation, increased safety, and reduced maintenance costs [1–4].

The need for global damage diagnosis has led to the development of methods that focus on detecting changes in a structure's vibration response characteristics as a result of changes in the dynamics caused by damage [2–7]. Most methods typically involve two phases: an initial *baseline (training) phase* which is performed once at outset, and under which the dynamics of the structure under healthy (and perhaps certain damage) conditions are obtained, and an *inspection phase* which may be performed on demand, or periodically, or even continuously in time (online), and under which the current structural dynamics are identified and "compared" in a proper sense to those of the baseline phase in order to achieve damage detection, localization and magnitude estimation.

Vibration based methods may be classified into two main subfamilies: (a) those based on detailed physical or analytical models (such as finite element models, FEMs) describing the complete structural dynamics and (b) those based on statistical time series and related methods. FEM based methods require the use of detailed "large" models, describing the complete structural dynamics, that need to be accurately updated in the inspection phase [3,8–13]. This is not only a burden for the inspection phase, but also an operation requiring a large number of installed sensors and measured signals [3,14,15].

Statistical time series and related methods offer the important advantage of being based on *partial* models of the structural dynamics, which are identified based on a potentially "small" number of vibration signals (sometimes even on a single signal or a single signal pair)—see the survey papers [5,6,16]. They may be thought of as generalizations of earlier techniques using deterministic models and identification techniques—a classical early approach being that of damage detection based on natural frequency changes in modal models [2,7,17]. Statistical time series type methods utilize statistical models and identification techniques that take uncertainties into account, they may operate on normal operating vibration signals, in an output-only mode, and also on structures of any size and geometry [18–23]. They may be thought of as including the related class of statistical pattern recognition type methods [24–29]. While damage detection may be potentially treated effectively by many of these methods, the damage localization problem is typically treated as a *classification problem*, meaning that a damage location is selected among a *finite* number of potential damage locations. This is a simplification, resulting in a much simpler problem than precise damage localization over properly defined *continuous topologies* on a structure – that is to say infinite possible damage locations – which essentially corresponds to the actual SHM problem. Furthermore, damage magnitude estimation is generally not possible (except for maybe some "rough" characterization)—a method offering an approach for properly tackling this problem has been recently introduced by the second author and co-workers [30,31].

The *aim* of the present study is the introduction and experimental validation and assessment of a generalized version of the FMBM which is – for the first time within the context of statistical time series type methods – achieving *complete* and *precise* damage *localization* over *continuous topologies* on a structure, combined with damage *magnitude estimation*. Furthermore, estimator uncertainties are fully taken into account in all phases of the diagnostic procedure, and uncertainty ellipsoids are provided for combined damage location and magnitude. Like the original FMBM, the method utilizes a partial and reduced size identified model, and is capable of operating on a "low" number of measurement sensors – even on a single pair for "small" structures – and any type of vibration response signals (acceleration, velocity, displacement).

The method's cornerstone is the new extended class of *vector-dependent functionally pooled* (VFP) models [32]. These are generalizations of the functional pooled (FP) models of Sakellariou and Fassois [30,33], which now allow for the analytical inclusion of *both* damage location and magnitude on the structural dynamics. VFP models thus allow for the extension of the notion of *damage mode* (fault mode) to include damage not only of all possible magnitudes, but also of all possible *locations* on a specific continuous topology on a structure. As VFP models have a richer structure than their FP counterparts and use bivariate (two-dimensional) polynomials belonging to functional subspaces for parameter projection, functional subspace dimensionality estimation is a more complicated task which is accomplished through a suitable genetic algorithm (GA) based procedure.

The method is validated and its effectiveness is experimentally assessed via a proof-of-concept application to damage detection, precise localization, and magnitude estimation on a prototype GARTEUR-type laboratory scale aircraft skeleton structure [34,35]. The damage scenarios considered include the attachment of varying size small masses to various continuous topologies on the structure. Such added mass "pseudo-faults" are often used in the literature as approximate ways of generating signals corresponding to various fault scenarios; for instance see [36–39]. In any case, the issue of using

added-mass type "pseudo-faults" is not of central importance in the present study, as the main goal is the development of the method and its validation by a simple proof-of-concept application.

The novelties achieved through this experimental study include:

(a) The feasibility of achieving *precise* damage localization and magnitude estimation based on only a *single* excitation–response signal pair is, for the first time, investigated and demonstrated.
(b) Localization and damage magnitude *uncertainties* are explicitly considered and estimated, with *uncertainty ellipsoids* corresponding to specified probability levels being constructed.
(c) The method's operation and effectiveness is examined for *both* "local" and "remote" (with respect to the sensor location) damages. This is critical in view of the need for effective diagnosis with the smallest possible number of available sensors.
(d) The effectiveness of the method in properly detecting and "negatively" localizing (that is excluding all considered structural topologies) damage that does *not* belong to any of the modeled types/topologies (referred to as *unmodeled damage*) is examined.

The rest of the paper is organized as follows: The proposed VFP-ARX model based method is presented in Section 3, and the experimental set-up used for validation and assessment is described in Section 4. Experimental results are provided in Section 5, while the conclusions are summarized in Section 6.

3. The VFP-ARX model based method

Like all statistical time series methods for SHM, the stochastic functional model, or more precisely the Vector-dependent Functionally Pooled AutoRegressive with eXogenous excitation (VFP-ARX) model based method, for combined damage detection, localization, and magnitude estimation consists of two phases: (a) A *baseline (training) phase*, which includes modeling of the considered damage topologies (modes), for the continuum of damage locations and magnitudes on a structural topology, via the novel class of stochastic VFP-ARX models, and (b) the *inspection phase*, which is performed whenever necessary or continuously during the structure's service cycle, and includes the functions of damage detection, localization, and magnitude estimation.

3.1. Baseline phase

3.1.1. Baseline modeling of the healthy structure

Although not strictly required, the modeling of the healthy (nominal) structure is an initial step performed in order to facilitate (in the sense of providing approximate model orders) the subsequent step of damage topology (mode) modeling.

A single experiment is performed, based on which an interval estimate of a discrete-time model (or a vector model or an array of models in the case of several vibration response measurement locations) representing the healthy structural dynamics is obtained via standard identification procedures [40–42]. In this study an array of two single excitation and single response AutoRegressive with eXogenous excitation (ARX) models is used.

An ARX(na,nb) model is of the form[1] [42]:

$$y[t]+\sum_{i=1}^{na} a_i \cdot y[t-i]=\sum_{i=0}^{nb} b_i \cdot x[t-i]+e[t], \quad e[t]\sim \text{iid}\ \mathcal{N}(0,\sigma_e^2) \tag{1}$$

with t designating the normalized discrete time ($t=1,2,3,\ldots$ with absolute time being $(t-1)T_s$, where T_s stands for the sampling period), $x[t]$, $y[t]$ the measured excitation and vibration response signals, respectively, na, nb the AutoRegressive (AR) and eXogenous (X) orders, respectively, and $e[t]$ the stochastic model residual (one-step-ahead prediction error) sequence, that is a white (serially uncorrelated), Gaussian, zero mean with variance σ_e^2 sequence, uncorrelated with the excitation $x[t]$. The symbol $\mathcal{N}(\cdot,\cdot)$ designates Gaussian distribution with the indicated mean and variance, and iid stands for identically independently distributed.

The model is parameterized in terms of the parameter vector $\overline{\boldsymbol{\theta}}=[a_i \vdots b_i \vdots \sigma_e^2]^T$ to be estimated from the measured signals [42,40]. Model estimation may be achieved based on minimization of the ordinary least squares (OLS) or the weighted least squares (WLS) criteria [42,40]. The modeling procedure involves the successive fitting of ARX(na,nb) models for increasing orders na and nb, until an adequate model is selected [42]. Model order selection is based on the Bayesian information criterion (BIC) and the residual sum of squares normalized by the series sum of squares (RSS/SSS). Final model validation is based on formal verification of the residual (one-step-ahead prediction error) sequence uncorrelatedness (whiteness) hypothesis [40, pp. 512–513].

[1] Lower case/capital bold face symbols designate vector/matrix quantities, respectively.

3.1.2. The notion of damage topology (mode)

The notion of *damage topology* (*mode*) refers to the union of all admissible damage magnitudes on a particular topology (section or component) of the structure (damage of all possible magnitudes at all possible locations along a topology). Hence, a damage topology is defined via two variables: (a) damage magnitude and (b) damage location. For this purpose, the novel stochastic Vector-dependent Functionally Pooled AutoRegressive with eXogenous excitation (VFP-ARX) models are used [32]. The VFP-ARX representation allows for complete and precise damage topology description, as the model parameters and residual series covariance depend functionally on damage magnitude and damage location, while the corresponding interrelations and statistical dependencies between the different damage magnitudes and locations are taken into account.

The VFP-ARX representation belongs to the recently introduced broader class of stochastic FP models, which make use of data pooling techniques for combining and optimally treating (as one entity) the data obtained from various experiments corresponding to different structural states and statistical techniques for model estimation [32,33,43].

3.1.3. Damage topology (mode) modeling

The modeling of a specific damage topology (mode) via a VFP-ARX model involves consideration of all admissible damage magnitudes occurring at predetermined locations on a specific section/component of the structure (right/left wing, horizontal stabilizer, and so on). For this reason a total of $M_1 \times M_2$ experiments is performed (physically or via analytical models and simulation), with M_1 and M_2 designating the number of experiments under the various damage magnitudes and locations, respectively. Each experiment is characterized by a specific damage magnitude k^1 and a specific damage location k^2, with the complete series covering the required range of each variable, say $[k^1_{min},\ k^1_{max}]$ and $[k^2_{min},\ k^2_{max}]$, via the discretizations $\{k^1_1,k^1_2,\ldots,k^1_{M_1}\}$ and $\{k^2_1,k^2_2,\ldots,k^2_{M_2}\}$ (it is tacitly assumed, without loss of generality, that the healthy structure corresponds to $k^1=0$). For the identification of a model corresponding to a specific damage topology the vector operating parameter $\boldsymbol{k}$ containing the damage magnitude and damage location components is defined as

$$\boldsymbol{k} \coloneqq [k^1_i \ \ k^2_j]^T \Leftrightarrow k_{i,j}, \quad i=1,\ldots,M_1,\ j=1,\ldots,M_2 \tag{2}$$

with $k_{i,j}$ designating the state of the structure corresponding to the i-th damage magnitude and the j-th damage location. This procedure yields a pool of excitation–response signal pairs (each of length N):

$$x_{\boldsymbol{k}}[t],y_{\boldsymbol{k}}[t] \quad \text{with } t=1,\ldots,N,\ k^1 \in \{k^1_1,\ldots,k^1_{M_1}\},\ k^2 \in \{k^2_1,\ldots,k^2_{M_2}\}. \tag{3}$$

A proper mathematical description of the structure for the considered damage topology may be then obtained in the form of a VFP-ARX model. In the case of several vibration measurement locations an array of such models (or else a vector model) may be obtained, with each scalar model corresponding to each measurement location and being designated as $\mathcal{M}^{XY}_{\boldsymbol{k}}$ (with X indicating the damage topology and Y the vibration measurement location).

The VFP-ARX model structure postulated is of the following form [32]:

$$y_{\boldsymbol{k}}[t]+\sum_{i=1}^{na} a_i(\boldsymbol{k})\cdot y_{\boldsymbol{k}}[t-i]=\sum_{i=0}^{nb} b_i(\boldsymbol{k})\cdot x_{\boldsymbol{k}}[t-i]+e_{\boldsymbol{k}}[t] \tag{4a}$$

$$e_{\boldsymbol{k}}[t]\sim \text{iid}\ \mathcal{N}(0,\sigma^2_e(\boldsymbol{k})), \quad \boldsymbol{k}\in\mathbb{R}^2 \tag{4b}$$

$$a_i(\boldsymbol{k}) \coloneqq \sum_{j=1}^{p} a_{i,j}\cdot G_j(\boldsymbol{k}), \quad b_i(\boldsymbol{k}) \coloneqq \sum_{j=1}^{p} b_{i,j}\cdot G_j(\boldsymbol{k}) \tag{4c}$$

$$E\{e_{k_{i,j}}[t]\cdot e_{k_{m,n}}[t-\tau]\}=\gamma_e[k_{i,j},k_{m,n}]\cdot\delta[\tau] \tag{4d}$$

with na, nb designating the AutoRegressive (AR) and eXogenous (X) orders, respectively, $x_{\boldsymbol{k}}[t]$, $y_{\boldsymbol{k}}[t]$ the excitation and response signals, respectively, and $e_{\boldsymbol{k}}[t]$ the model's residual (one-step-ahead prediction error) sequence, that is a white (serially uncorrelated) zero mean sequence with variance $\sigma^2_e(\boldsymbol{k})$. This sequence should be uncorrelated with the excitation $x_{\boldsymbol{k}}[t]$ but potentially cross-correlated with its counterparts corresponding to different experiments (different $\boldsymbol{k}$'s). The symbol $E\{\cdot\}$ designates statistical expectation, $\delta[\tau]$ the Kronecker delta (equal to unity for $\tau=0$ and equal to zero for $\tau\neq 0$), $\mathcal{N}(\cdot,\cdot)$ Gaussian distribution with the indicated mean and variance, and iid stands for identically independently distributed.

As (4c) indicates, the AR and X parameters $a_i(\boldsymbol{k})$, $b_i(\boldsymbol{k})$ are modeled as explicit functions of the vector $\boldsymbol{k}$ (which contains the damage magnitude and damage location components) by belonging to p-dimensional functional subspace spanned by the mutually independent basis functions $G_1(\boldsymbol{k}),G_2(\boldsymbol{k}),\ldots,G_p(\boldsymbol{k})$ (*functional basis*). The functional basis consists of polynomials of two variables (bivariate) obtained as tensor products from their corresponding univariate polynomials (Chebyshev, Legendre, Jacobi, and other families [44]), while the whole procedure of the subspace creation is described in detail in Appendix A. The constants $a_{i,j}$ and $b_{i,j}$ designate the AR and X, respectively, coefficients of projection.

The VFP-ARX model of (4a)–(4d) is parameterized in terms of the parameter vector to be estimated from the measured signals:

$$\overline{\boldsymbol{\theta}} \coloneqq [\alpha_{i,j} \ \vdots\ b_{i,j} \ \vdots\ \sigma^2_e(\boldsymbol{k})]^T \quad \forall\, \boldsymbol{k} \tag{5}$$

and may be written in linear regression form as

$$y_{\boldsymbol{k}}[t] = [\boldsymbol{\varphi}_{\boldsymbol{k}}^T[t] \otimes \boldsymbol{g}^T(\boldsymbol{k})] \cdot \boldsymbol{\theta} + e_{\boldsymbol{k}}[t] = \boldsymbol{\varphi}_{\boldsymbol{k}}^T[t] \cdot \boldsymbol{\theta} + e_{\boldsymbol{k}}[t] \tag{6}$$

with

$$\boldsymbol{\varphi}_{\boldsymbol{k}}[t] \coloneqq [-y_{\boldsymbol{k}}[t-1] \ldots -y_{\boldsymbol{k}}[t-na] \vdots x_{\boldsymbol{k}}[t] \ldots x_{\boldsymbol{k}}[t-nb]]_{[(na+nb+1)\times 1]}^T \tag{7a}$$

$$\boldsymbol{g}(\boldsymbol{k}) \coloneqq [G_1(\boldsymbol{k}) \ldots G_p(\boldsymbol{k})]_{[p\times 1]}^T \tag{7b}$$

$$\boldsymbol{\theta} \coloneqq [a_{1,1} \ldots a_{na,p} \vdots b_{0,1} \ldots b_{nb,p}]_{[(na+nb+1)p\times 1]}^T \tag{7c}$$

and ^{T} designating transposition and $\otimes$ Kronecker product [45, Chapter 7].

Pooling together the expressions (6) of the VFP-ARX model corresponding to all vector operating parameters $\boldsymbol{k}$ $(k_{1,1}, k_{1,2}, \ldots, k_{M_1,M_2})$ considered in the experiments (cross-sectional pooling) yields

$$\begin{bmatrix} y_{k_{1,1}}[t] \\ \vdots \\ y_{k_{M_1,M_2}}[t] \end{bmatrix} = \begin{bmatrix} \boldsymbol{\phi}_{k_{1,1}}^T[t] \\ \vdots \\ \boldsymbol{\phi}_{k_{M_1,M_2}}^T[t] \end{bmatrix} \cdot \boldsymbol{\theta} + \begin{bmatrix} e_{k_{1,1}}[t] \\ \vdots \\ e_{k_{M_1,M_2}}[t] \end{bmatrix} \Rightarrow \boldsymbol{y}[t] = \boldsymbol{\Phi}[t] \cdot \boldsymbol{\theta} + \boldsymbol{e}[t]. \tag{8}$$

Then, following substitution of the data for $t=1,\ldots,N$ the following expression is obtained:

$$\boldsymbol{y} = \boldsymbol{\Phi} \cdot \boldsymbol{\theta} + \boldsymbol{e} \tag{9}$$

with

$$\boldsymbol{y} \coloneqq \begin{bmatrix} \boldsymbol{y}[1] \\ \vdots \\ \boldsymbol{y}[N] \end{bmatrix}, \quad \boldsymbol{\Phi} \coloneqq \begin{bmatrix} \boldsymbol{\Phi}[1] \\ \vdots \\ \boldsymbol{\Phi}[N] \end{bmatrix}, \quad \boldsymbol{e} \coloneqq \begin{bmatrix} \boldsymbol{e}[1] \\ \vdots \\ \boldsymbol{e}[N] \end{bmatrix}. \tag{10}$$

Using the above linear regression framework the simplest approach for estimating the projection coefficient vector $\boldsymbol{\theta}$ is based on minimization of the ordinary least squares (OLS) criterion $J^{\mathrm{OLS}} \coloneqq (1/N)\sum_{t=1}^{N} \boldsymbol{e}^T[t]\boldsymbol{e}[t]$.

A more appropriate criterion is (in view of the Gauss–Markov theorem [46]) the weighted least squares (WLS) criterion:

$$J^{\mathrm{WLS}} \coloneqq \frac{1}{N}\sum_{t=1}^{N} \boldsymbol{e}^T[t]\boldsymbol{\Gamma}_{\boldsymbol{e}[t]}^{-1}\boldsymbol{e}[t] = \frac{1}{N}\boldsymbol{e}^T\boldsymbol{\Gamma}_{\boldsymbol{e}}^{-1}\boldsymbol{e} \tag{11}$$

which leads to the *weighted least squares* (WLS) estimator:

$$\widehat{\boldsymbol{\theta}}^{\mathrm{WLS}} = [\boldsymbol{\Phi}^T\boldsymbol{\Gamma}_{\boldsymbol{e}}^{-1}\boldsymbol{\Phi}]^{-1}[\boldsymbol{\Phi}^T\boldsymbol{\Gamma}_{\boldsymbol{e}}^{-1}\boldsymbol{y}] \tag{12}$$

In these expressions $\boldsymbol{\Gamma}_{\boldsymbol{e}} = E\{\boldsymbol{e}\boldsymbol{e}^T\}$ ($\boldsymbol{\Gamma}_{\boldsymbol{e}} = \boldsymbol{\Gamma}_{\boldsymbol{e}[t]} \otimes \boldsymbol{I}_N$, with $\boldsymbol{I}_N$ designating the $N \times N$ unity matrix) designates the residual covariance matrix, which is practically unavailable. Nevertheless, it may be consistently estimated by applying (in an initial step) ordinary least squares (details in [32]). Once $\widehat{\boldsymbol{\theta}}^{\mathrm{WLS}}$ has been obtained, the final residual variance and residual covariance matrix estimates are obtained as

$$\widehat{\sigma}_e^2(\boldsymbol{k}, \widehat{\boldsymbol{\theta}}^{\mathrm{WLS}}) = \frac{1}{N}\sum_{t=1}^{N} e_{\boldsymbol{k}}^2[t, \widehat{\boldsymbol{\theta}}^{\mathrm{WLS}}], \quad \widehat{\boldsymbol{\Gamma}}_{\boldsymbol{e}[t]} = \frac{1}{N}\sum_{t=1}^{N} \boldsymbol{e}[t, \widehat{\boldsymbol{\theta}}^{\mathrm{WLS}}]\boldsymbol{e}^T[t, \widehat{\boldsymbol{\theta}}^{\mathrm{WLS}}]. \tag{13}$$

The estimator $\widehat{\boldsymbol{\theta}}^{\mathrm{WLS}}$ may, under mild conditions, be shown to be asymptotically Gaussian distributed with mean coinciding with the true parameter vector $\boldsymbol{\theta}^0$ and covariance matrix $\boldsymbol{P}_{\boldsymbol{\theta}}$:

$$\sqrt{N}(\widehat{\boldsymbol{\theta}}_N - \boldsymbol{\theta}^0) \sim \mathcal{N}(\boldsymbol{0}, \boldsymbol{P}_{\boldsymbol{\theta}}) \quad (N \to \infty) \tag{14}$$

based on which interval estimates of the true parameter vector may be constructed [32].

The problem of VFP-ARX model structure selection (structure estimation) for a given basis function family (such as Chebyshev, Legendre, and so on), that is model order determination for the AR and X polynomials and determination of their corresponding functional subspaces, is referred to as the model identification problem. Usually, the AR and X model orders are initially selected via customary model order selection techniques (BIC, RSS, stabilization diagrams) [40], whereas the functional subspace dimensionalities are selected via a genetic algorithm (GA) procedure [47]. Initially, maximum functional subspace dimensionalities are selected, which define the search space of the functional subspace estimation subproblem. The determination of the exact subspace dimensionalities is achieved via the use of GAs based on minimization of the BIC with respect to the candidate basis functions.

3.2. Inspection phase

Let $x[t]$, $y[t]$ $(t = 1,2,\ldots,N)$ represent the current excitation and response signals, respectively, obtained from the structure in an *unknown* (to be classified) state. Damage detection, localization, and magnitude estimation are based on the

pre-determined (in the baseline phase) VFP-ARX models, with each model corresponding to a specific damage topology (mode). The current excitation and response signals are driven through these models and estimates of the current values of the operating vector $\boldsymbol{k}$ and residual series $e_{\boldsymbol{k}}[t]$ are obtained from each one. These estimates are subsequently used for tackling the damage detection, localization, and magnitude estimation tasks within a statistical decision making framework.

3.2.1. Step I: damage detection

Damage detection is based on the re-parameterized, in terms of $\boldsymbol{k}$ and $\sigma_e^2(\boldsymbol{k})$ VFP-ARX model of *any* damage topology (e.g. *V*). Thus, the projection coefficients are replaced by the corresponding estimates available from the baseline phase, while the vector $\boldsymbol{k}$ containing the damage magnitude and location, and the residual series variance $\sigma_e^2(\boldsymbol{k})$ are the current unknown parameters to be estimated:

$$\mathcal{M}^V(\boldsymbol{k},\sigma_e^2(\boldsymbol{k})) : y[t]+\sum_{i=1}^{na} a_i(\boldsymbol{k})\cdot y[t-i]=\sum_{i=0}^{nb} b_i(\boldsymbol{k})\cdot x[t-i]+e[t]. \tag{15}$$

The estimation of the currently unknown parameters $\boldsymbol{k}$ and $\sigma_e^2(\boldsymbol{k})$ based on the current excitation and response signals may be achieved via the following nonlinear least squares (NLS) and variance estimators (refer to [40, pp. 327–329] for details on NLS estimation):

$$\widehat{\boldsymbol{k}}=\arg\min_{\boldsymbol{k}} \sum_{t=1}^{N} e^2[t], \quad \sigma_e^2(\widehat{\boldsymbol{k}})=\frac{1}{N}\sum_{t=1}^{N} e^2[t,\widehat{\boldsymbol{k}}] \tag{16}$$

the first one realized via a hybrid optimization scheme based on genetic algorithms (GA) [47] and constrained nonlinear optimization (sequential quadratic programming—SQP) [48,49].

The GA aims at exploring the complete search space ((k^1,k^2) plane) with the objective of locating promising regions within which the "true" $\boldsymbol{k}$ might be located. Despite the GA's inherent ability for effective global optimization, they often suffer in terms of exact global optimum localization. Hence, a constrained nonlinear optimization scheme is employed in a suitably defined neighborhood of the GA result in order to find the exact global optimum $\widehat{\boldsymbol{k}}$.

Assuming that the structure is indeed under a damage belonging to damage topology *V* (or healthy) the first estimator may be shown to be asymptotically ($N\to\infty$) Gaussian distributed, with mean equal to the true $\boldsymbol{k}$ value and covariance matrix $\boldsymbol{\Sigma}_{\boldsymbol{k}}$ ($\widehat{\boldsymbol{k}}\sim\mathcal{N}(\boldsymbol{k},\boldsymbol{\Sigma}_{\boldsymbol{k}})$) coinciding with the Cramer–Rao lower bound, which may be obtained as

$$\widehat{\boldsymbol{\Sigma}}_{\boldsymbol{k}}=\frac{\widehat{\sigma}_e^2(\widehat{\boldsymbol{k}})}{N}\left[\frac{1}{N}\sum_{t=1}^{N}\left[\boldsymbol{\varphi}^T[t]\otimes\frac{\partial \boldsymbol{g}^T(\boldsymbol{k})}{\partial \boldsymbol{k}}\bigg|_{\boldsymbol{k}=\widehat{\boldsymbol{k}}}\cdot\widehat{\boldsymbol{\theta}}\right]\cdot\left[\boldsymbol{\varphi}^T[t]\otimes\frac{\partial \boldsymbol{g}^T(\boldsymbol{k})}{\partial \boldsymbol{k}}\bigg|_{\boldsymbol{k}=\widehat{\boldsymbol{k}}}\cdot\widehat{\boldsymbol{\theta}}\right]^T\right]^{-1}. \tag{17}$$

In this expression $\boldsymbol{\varphi}[t]$ is defined as in (7a), while $\widehat{\boldsymbol{\theta}}$ designates the available from the baseline phase estimate of projection coefficients vector corresponding to the selected damage topology model.

Since the healthy structure corresponds to $k^1=0$ (zero damage magnitude) for any damage topology model, damage detection may be based on the following hypothesis testing problem:

$$\begin{aligned} &H_0 : k^1=0 \text{ (null hypothesis}-\text{healthy structure)}\\ &H_1 : k^1\neq 0 \text{ (alternative hypothesis}-\text{damaged structure).}\end{aligned} \tag{18}$$

Under the null (H_0) hypothesis, the following statistic follows *t*-distribution with $N-1$ degrees of freedom (which should be adjusted to $N-2$ in case the estimated mean is subtracted from the residual series in the computation of $\widehat{\boldsymbol{\Sigma}}_{\boldsymbol{k}}$):

$$t=\frac{\widehat{k}^1}{\widehat{\sigma}_{k^1}}\sim t(N-1) \tag{19}$$

with $\widehat{\sigma}_{k^1}$ being the positive square root of the first diagonal element of $\widehat{\boldsymbol{\Sigma}}_{\boldsymbol{k}}$ (estimated standard deviation of k^1). This leads to the following test at the α risk level (probability of false alarm, or type I error, that is accepting H_1 although H_0 is true, being equal to α):

$$\begin{aligned} &t_{\alpha/2}(N-1)\le t\le t_{1-\alpha/2}(N-1)\Rightarrow H_0 \text{ is accepted (healthy structure)}\\ &\text{Else}\Rightarrow H_1 \text{ is accepted (damaged structure)}\end{aligned} \tag{20}$$

with t_α designating the *t* distribution's (with the indicated degrees of freedom) α critical point [defined such that $\text{Prob}(t\le t_\alpha)=\alpha$].

3.2.2. Step II: damage topology (mode) identification

Damage topology (mode) identification corresponds to the examination of which one of the available damage topology VFP-ARX models provides, for its estimated $\widehat{\boldsymbol{k}}$, a valid representation of the *current* structural dynamics based on residual uncorrelatedness (whiteness) hypothesis testing. The current damage topology is that corresponding to the valid model, which will exhibit an uncorrelated (white) residual sequence for the corresponding $\widehat{\boldsymbol{k}}$.

Once damage occurrence has been detected, current damage topology determination is based on the successive estimation (using the current data) and validation of the re-parameterized $\mathcal{M}^V(\boldsymbol{k},\sigma_e^2(\boldsymbol{k}))$ VFP-ARX models (Eq. (15)) for $V=A,B,\ldots$ corresponding to the various damage modes. The procedure stops as soon as a particular model is successfully validated, with the corresponding damage topology identified as current. Model validation may be based on a statistical test examining the residual uncorrelatedness (whiteness) via the statistical hypothesis testing problem:

$$\begin{aligned} &H_0 : \rho_V[\tau]=0 \quad \tau=1,2,\ldots,r \text{ (damage is of type } V)\\ &H_1 : \rho_V[\tau]\neq 0 \quad \text{for some } \tau \text{ (damage is not of type } V) \end{aligned} \tag{21}$$

in which $\rho_V[\tau]$ ($\tau=1,2,\ldots,r$) designates the residual series normalized autocorrelation at lag τ. Under the null hypothesis the following Q statistic follows a chi-square (χ^2) distribution with r degrees of freedom [50, p. 314]:

$$Q=N(N+2)\cdot\sum_{\tau=1}^{r}(N-\tau)^{-1}\widehat{\rho}_V^2[\tau]\sim\chi^2(r) \tag{22}$$

in which N designates the residual signal length (in number of samples), $\widehat{\rho}_V[\tau]$ the estimated (sample) normalized autocorrelation at lag τ, and r the maximum lag. This leads to the following test at the α risk level:

$$\begin{aligned} &Q<\chi^2_{1-\alpha}(r)\Rightarrow H_0 \text{ is accepted (damage is of type } V)\\ &\text{Else}\Rightarrow H_1 \text{ is accepted (damage is not of type } V) \end{aligned} \tag{23}$$

with $\chi^2_{1-\alpha}(r)$ designating the distribution's $(1-\alpha)$ critical point.

It should be noticed that inability to identify a particular damage topology (obviously as not previously modeled) indirectly implies damage detection.

3.2.3. *Step III: damage localization and magnitude estimation*

Damage localization and magnitude estimation are then based on the interval estimates of k^2 and k^1, respectively, which are constructed based on the $\widehat{\boldsymbol{k}}$, $\widehat{\boldsymbol{\Sigma}}_{\boldsymbol{k}}$ estimates obtained from the corresponding re-parameterized VFP-ARX model (of the form (15)) of the *current* valid damage topology. Thus, using (19), the interval estimates of k^1 (damage magnitude) and k^2 (damage location) at the α risk level are

$$k^i \text{ interval estimate}: \ [\widehat{k}^i-t_{\frac{\alpha}{2}}(N-1)\cdot\widehat{\sigma}_{k^i},\widehat{k}^i+t_{1-\frac{\alpha}{2}}(N-1)\cdot\widehat{\sigma}_{k^i}] \tag{24}$$

with $i=1$ for damage magnitude and $i=2$ for damage location, while $\widehat{\sigma}_{k^i}$ is the positive square root of the i-th diagonal element of $\widehat{\boldsymbol{\Sigma}}_{\boldsymbol{k}}$.

Bivariate confidence bounds for $\boldsymbol{k}=[k^1\ k^2]^T$ may be also obtained by observing that the quantity follows chi-square distribution with two degrees of freedom [40, p. 558]:

$$(\widehat{\boldsymbol{k}}-\boldsymbol{k})^T\boldsymbol{\Sigma}_{\boldsymbol{k}}^{-1}(\widehat{\boldsymbol{k}}-\boldsymbol{k})\sim\chi^2_{1-\alpha}(2). \tag{25}$$

Thus the probability that

$$(\widehat{\boldsymbol{k}}-\boldsymbol{k})^T\boldsymbol{\Sigma}_{\boldsymbol{k}}^{-1}(\widehat{\boldsymbol{k}}-\boldsymbol{k})\leq\chi^2_{1-\alpha}(2) \tag{26}$$

is equal to $1-\alpha$ ($\chi^2_{1-\alpha}(2)$ designating the χ^2 distribution's with two degrees of freedom $1-\alpha$ critical point). This expression defines an ellipsoid on the (k^1,k^2) plane within which the true (k^1,k^2) point should lie with probability $(1-\alpha)$, or equivalently, with risk α (*bivariate confidence bounds*). The shape of the ellipsoid is determined by $\boldsymbol{\Sigma}_{\boldsymbol{k}}$. Notice that in

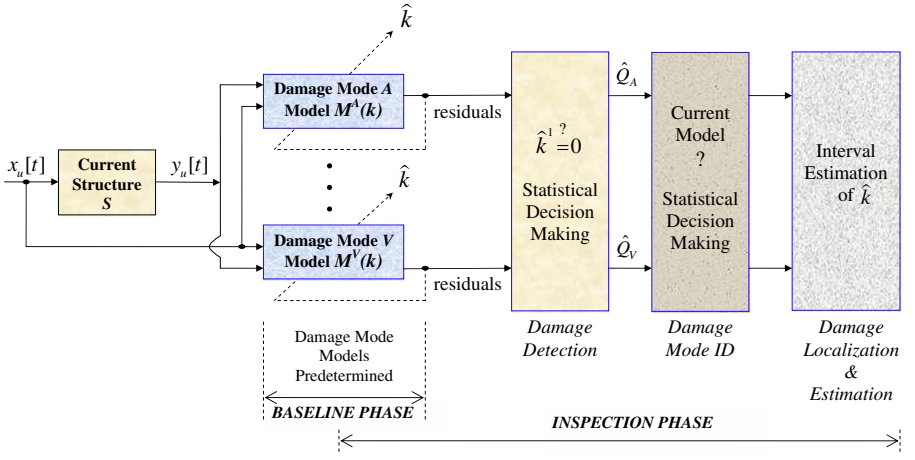

Fig. 1. Flowchart representation of the VFP-ARX model based method.

practice $\boldsymbol{\Sigma}_{\boldsymbol{k}}$ is replaced by its estimate, which is assumed to be of negligible variability.

Fig. 1 presents a flowchart representation of the VFP-ARX model based method.

4. The experimental set-up

4.1. The structure

The scale aircraft skeleton structure used in the experiments was designed by ONERA (France) in conjunction with the Structures and Materials Action Group SM-AG19 of the Group for Aeronautical Research and Technology in Europe (GARTEUR) [34,35]. The currently used structure has been manufactured at the University of Patras (Fig. 2a). This testbed represents a typical aircraft skeleton design and consists of six solid beams with rectangular cross sections representing the fuselage, the wing, the horizontal and vertical stabilizers, and the right and left wing tips. All parts of the structure are constructed from standard aluminum and are jointed together via steel plates and screws. The total mass of the structure is approximately 50 kg and its dimensions are indicated in Table 1.

4.2. The damage topologies and scenarios

The damage scenarios considered correspond to the attachment of a variable number of small unit masses, simulating local elasticity reductions, at three different topologies (presently geometrical axes) on the structure. Each unit mass weighs approximately 8.132 g and is attached to the structure using adhesive wax. As already mentioned in Section 2, such added mass "pseudo-faults" are often used in the literature as approximate ways of generating signals corresponding to various fault scenarios; for instance see [30,36–39]. Other types of damages, such as the loosening of bolts, have been also

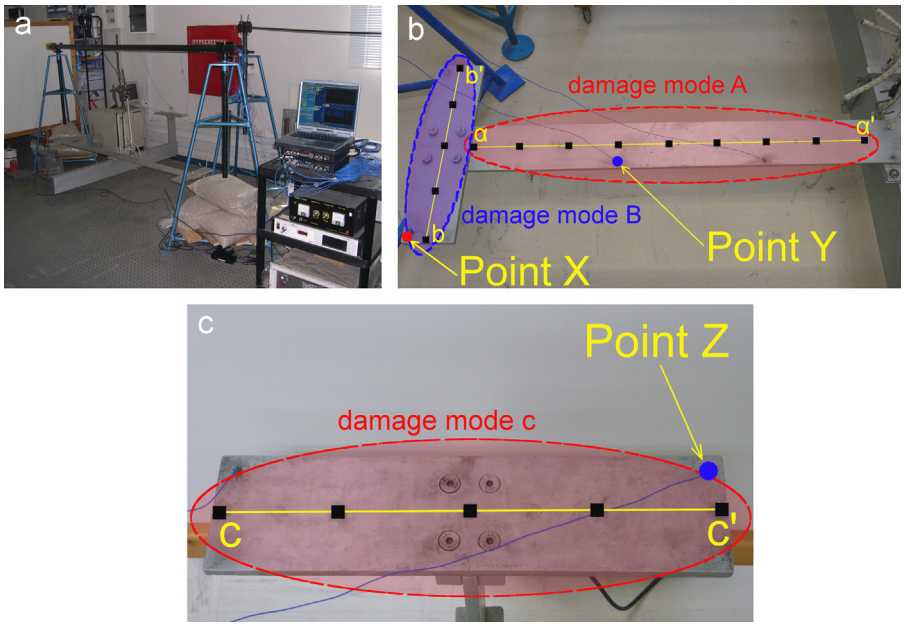

Fig. 2. (a) The scale aircraft skeleton structure and the experimental set-up; (b) the right wing-tip with the force excitation (Point X), the first vibration measurement position (Point Y), and the aa' and bb' axes that define the A and B damage topologies, respectively; (c) the horizontal stabilizer with the second vibration measurement position (Point Z) and the cc' axis that defines the C damage topology.

Table 1
Dimensions of the scale aircraft skeleton structure.

Component	Length (mm)	Width (mm)	Thickness (mm)
Fuselage	1500	150	50
Wings	2000	100	10
Horizontal stabilizer	300	100	10
Vertical stabilizer	400	100	10
Wing-tips	400	100	10

Table 2
The considered damage topologies (modes)—refer to Fig. 2b–c.

Damage topology (mode)	Description
A	Any mass anywhere on the right wing ($k^1 \in [0,81.32]$ g, $k^2 \in [0,80]$ cm)
B	Any mass anywhere on the right wing-tip ($k^1 \in [0,81.32]$ g, $k^2 \in [0,40]$ cm)
C	Any mass anywhere on the hor. stab. ($k^1 \in [0,81.32]$ g, $k^2 \in [0,40]$ cm)

Table 3
Signal pre-processing and details.

Sampling frequency: $f_s=256$ Hz	Bandwidth: [4–90] Hz
Signal length: $N=1500$ samples (5.85 s)	

effectively considered – with similar results – in other recent studies [51,52]. In any case the issue of "pseudo-faults" used in the training (baseline) phase is not of central importance in the present study, which focuses on the development of the method and its validation by a simple proof-of-concept application.

In the context of this study each damage belongs to one of three distinct *damage topologies* (modes) (see Fig. 2 and Table 2):

(a) The first (*damage topology* (*mode*) *A*) corresponds to the attachment of up to 10 unit masses at a single location, representing different damage magnitudes in the range of [0,81.32] g, at any point on the aa' axis (Fig. 2b), starting from a and moving to the left along the right wing of the aircraft in the range 0–80 cm— Fig. 2.
(b) The second (*damage topology* (*mode*) *B*) corresponds to the attachment of up to 10 unit masses at a single location, representing different damage magnitudes in the range of [0,81.32] g, at any point on the bb' axis (Fig. 2b), starting from b and moving backwards along the right wing-tip in the range 0–40 cm.
(c) The third (*damage topology* (*mode*) *C*) corresponds to the attachment of up to 10 unit masses at a single location, representing different damage magnitudes in the range of [0,81.32] g, at any point on the cc' axis (Fig. 2c), starting from c and moving to the left along the horizontal stabilizer in the range 0–40 cm.

Each damage – belonging to any one of the above topologies or, perhaps, to an "unmodeled" topology – is designated as $F^X_{k^1,k^2}$, with X=A, B, C indicating a particular damage topology, k^1 the damage magnitude (g of added mass) and k^2 the precise damage location (distance in cm) along the pertinent axis. The healthy structure corresponds to $k^1=0$ (0 g of added mass) and is designated as F_o.

4.3. The experimental procedure

Damage detection, localization, and magnitude estimation are based on vibration testing of the structure, which is suspended through a set of bungee cords and hooks from a long rigid beam sustained by four heavy-type stands (Fig. 2a). The suspension is designed in a way as to exhibit a pendulum rigid body mode below the frequency range of interest, as the boundary conditions are free–free.

The excitation is broadband random stationary Gaussian applied vertically at the right wing-tip (Point X, Fig. 2b) through an electromechanical modal shaker (MB Dynamics Modal 50A, max load 225 N) equipped with a stinger. The actual force exerted on the structure is measured via an impedance head (PCB M288D01, sensitivity 98.41 mV/lb), while the resulting vertical acceleration responses at Points Y and Z (Fig. 2b–c) are measured via lightweight accelerometers (PCB 352A10 miniature ICP accelerometers, 0.7 g, frequency range 0.003–10 kHz, sensitivity ~ 1.052 mV/m/s^2). The force and acceleration signals are driven through a conditioning charge amplifier (PCB 481A02) into the data acquisition system based on SigLab 20-42 measurement modules (each module featuring four 20-bit simultaneously sampled A/D channels, two 16-bit D/A channels, and analog anti-aliasing filters).

4.4. The signals

The excitation and response signal bandwidth is selected as 4–90 Hz, with the lower limit set in order to avoid instrument dynamics and rigid body modes. Each signal is digitized at $f_s=256$ Hz, resulting in a length of $N=1500$ samples, and is subsequently sample mean corrected and normalized by its sample standard deviation (Table 3).

Table 4
The considered test cases[a].

Test case	Damage	Damage topology (mode)	Description
I	F_o	–	Healthy structure
II	$F^A_{8.132,80}$	A	Mass of 8.132 g at 80 cm (right wing)
III	$F^A_{32.528,0}$	A	Mass of 32.528 g at 0 cm (right wing)
IV	$F^A_{40.66,75}$	A	Mass of 40.66 g at 75 cm (right wing)
V	$F^B_{8.132,0}$	B	Mass of 8.132 g at 0 cm (right wing-tip)
VI	$F^B_{16.26,5}$	B	Mass of 16.26 g at 5 cm (right wing-tip)
VII	$F^C_{12.19,10}$	C	Mass of 12.19 g at 10 cm (horizontal stab.)
VIII	$F^C_{81.32,30}$	C	Mass of 81.32 g at 30 cm (horizontal stab.)
IX	$F_{40.66,10}$	Unmodeled	Mass of 40.66 g at 10 cm (left wing-tip)

[a] Each case is considered separately via Point Y and Point Z measurements.

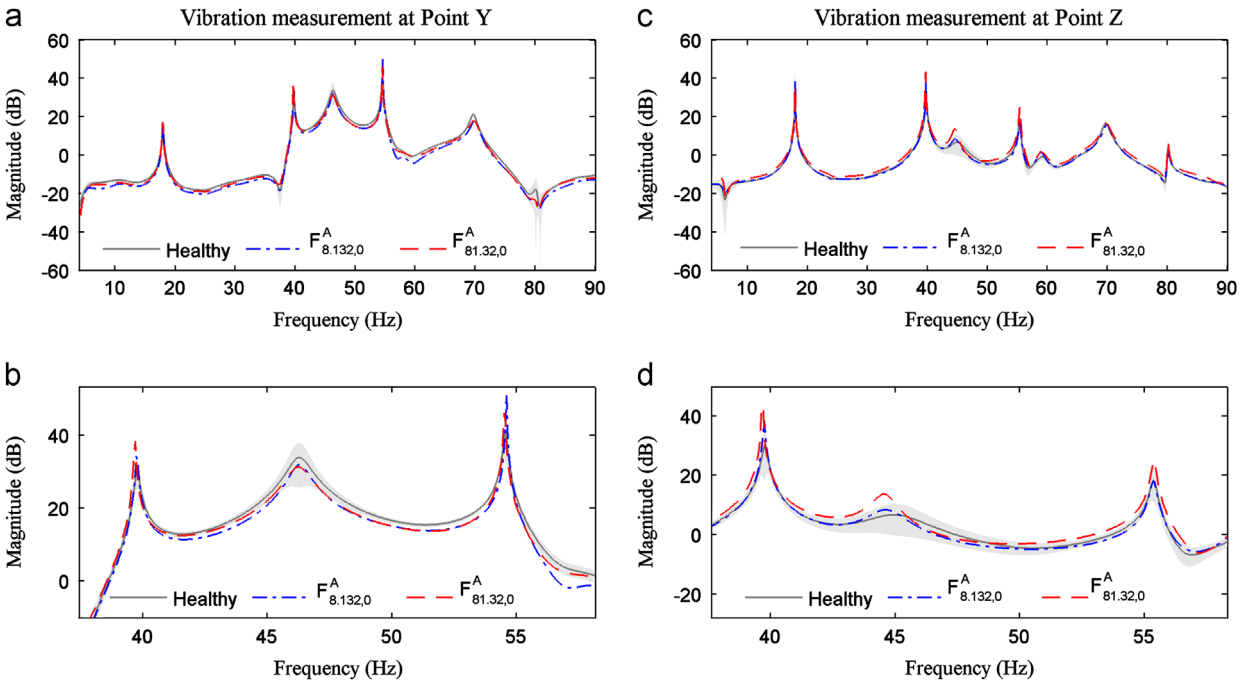

Fig. 3. The effects of two topology A damages on parametrically obtained FRF magnitude curves corresponding to each one of the Point X–Point Y (a–b) and Point X–Point Z (c–d) transfer functions. The gray zones depict 95% confidence intervals (uncertainty zones) for the healthy FRF magnitudes. The (b) and (d) subplots are blow ups of (a) and (c), respectively.

5. Damage detection, localization, and magnitude estimation results

Damage detection, localization, and magnitude estimation results for damage of any magnitude occurring anywhere in one of the three specified *topologies* (modes) are now presented.

The considered damage test cases are summarized in Table 4—each test case is considered twice, first via the Point Y and then via the Point Z sensor. Notice that Test Case I corresponds to the healthy structure, Test Cases II–IV to damage in topology A (right wing), Test Cases V–VI to damage in topology B (right wing-tip), Test Cases VII–VIII to damage in topology C (horizontal stabilizer), while Test Case IX does *not* belong to any of the considered topologies and for this reason it is referred to as "unmodeled" (it corresponds to damage on the left wing-tip). The challenging issue with this last Test Case is whether or not it will be possible to detect it and "negatively" localize it as not belonging to any one of the A–C topologies. It should be further emphasized that none of the damages considered in the Test Cases is used in the baseline (training) phase of the next subsection.

The damage diagnosis method operates on a single pair of excitation–response signals, namely the excitation force that is always applied at Point X, and a vibration acceleration response measured either at Point Y or at Point Z (Fig. 2b–c).

Depending on the distance of the employed accelerometer sensor from the damage occurrence location, the damage is labeled as being "*local*" or "*remote*" to the response sensor used.

The effects of the considered damage cases to the structural dynamics are depicted in Fig. 3, which presents parametric (ARX(48, 48) model based) frequency response function (FRF) magnitude estimates (Matlab function *ffplot.m*) for the Point X–Point Y and Point X–Point Z transfer functions for the healthy and two damage cases belonging to topology (mode) A (notice that 95% confidence intervals are also depicted for the healthy FRFs). Evidently, the effects of damage are rather small, which underscores the challenges underlying the damage diagnosis problem.

5.1. Baseline phase

5.1.1. Baseline modeling of the healthy structure

Conventional ARX models representing the healthy structure are obtained through standard identification procedures [42,40] based on obtained excitation–response signals (5.85 s, $N=1500$ sample long, Matlab function *arx.m*). This leads to an ARX(48, 48) model characterized by zero delay ($b_0 \neq 0$ in the exogenous polynomial) for the Point X–Point Y transfer function. Similarly, an ARX(51, 51) model ($b_0 \neq 0$) is obtained for the Point X–Point Z transfer function. These models are used as reference and for providing approximate orders for the corresponding damage topology (mode) models of the next paragraph.

5.1.2. Modeling of the dynamics for damage topologies (modes) A, B, C

Damage mode modeling for damage topology (mode) A (right wing—refer to Table 2) is based on signals obtained from a total of $M_1 \times M_2 = 99$ experiments. Nine experiments correspond to the healthy structure ($k^1 = 0$ g) and 90 to the damaged structure (1–10 unit masses being placed at each one of nine locations on the right wing— Fig. 2b). The mass and location increments used are $\delta k^1 = 8.132$ g and $\delta k^2 = 10$ cm, covering the intervals [0,81.32] g and [0, 80] cm.

Damage mode modeling for damage topologies (modes) B (right wing-tip) and C (horizontal stabilizer) (refer to Table 2) is based on signals obtained from a total of $M_1 \times M_2 = 55$ experiments. Five experiments correspond to the healthy structure ($k^1 = 0$ g) and 50 to the damaged structure (1–10 unit masses being placed at each one of five locations on the right wing-tip for damage mode B or on the horizontal stabilizer for damage mode C— Fig. 2b–c). The mass and location increments used are $\delta k^1 = 8.132$ g and $\delta k^2 = 10$ cm, covering the intervals [0, 81.32] g and [0, 40] cm.

Based on the signals collected from the aforementioned experiments, two models are identified for each one of the A, B, C damage topologies: the first model describes the Point X–Point Y dynamics (transfer function) and the second the Point X–Point Z dynamics (transfer function).

Model order selection starts with the orders selected for the conventional ARX models representing the healthy structure, the final model orders being presently selected based on the BIC criterion [42] and model validation techniques, such as checking the whiteness (uncorrelatedness) and the normality of the model residuals (Matlab functions *acf.m* and *normplot.m*, respectively) [42,40]. The functional subspaces are selected via a genetic algorithm (GA) based procedure (Matlab function *ga.m*). An extended functional subspace consisting of 45 Chebyshev Type II bivariate polynomial basis functions (see Appendix A) is initially considered, with the GA aiming at selecting the optimal functional basis subset based on BIC minimization (see Appendix B—GA estimation details in Table 7).

The identified damage topology models are summarized in Table 6 and are as follows:

(a) Point X–Point Y dynamics: A VFP-ARX damage model is identified for each damage topology based on $N=1500$ sample-long signals: a VFP-ARX(48, 48) for damage topology A, a VFP-ARX(57, 57) for damage topology B, and a VFP-ARX(44, 44) model for damage topology C. Each functional subspace consists of $p=30$ Chebyshev Type II two-dimensional polynomials.

(b) Point X–Point Z dynamics: A VFP-ARX damage model is identified for each damage topology based on $N=1500$ sample-long signals: a VFP-ARX(51, 51) for damage topology A, a VFP-ARX(69, 69) for damage topology B, and a VFP-ARX(65, 65) model for damage topology C. Like in the previous case, each functional subspace consists of $p=30$ Chebyshev Type II two-dimensional polynomials.

Indicative FRF magnitude curves obtained from damage topology A and the Point Y VFP$-$ARX$(48,48)_{30}$ model (designated as $\mathcal{M}_{\boldsymbol{k}}^{AY}$) are, as functions of frequency, damage magnitude and location, depicted in Fig. 4. Indicative AR parameters of the same model are depicted in Fig. 5 as functions of damage magnitude and location. Similarly, indicative natural frequencies obtained by the model as functions of damage magnitude and location are presented in Fig. 6 (also compare with Fig. 3 and Table 5).

5.2. Inspection phase: damage detection, localization and magnitude estimation

The effectiveness of the damage diagnosis method is now assessed via the Test Cases of Table 4. It should be stressed that the damages associated with the Test Cases do *not* coincide with those used in the baseline (training) phase—apart from Test Case I that corresponds to the healthy structure. Each one of the first eight Test Cases (I–VIII) is considered twice:

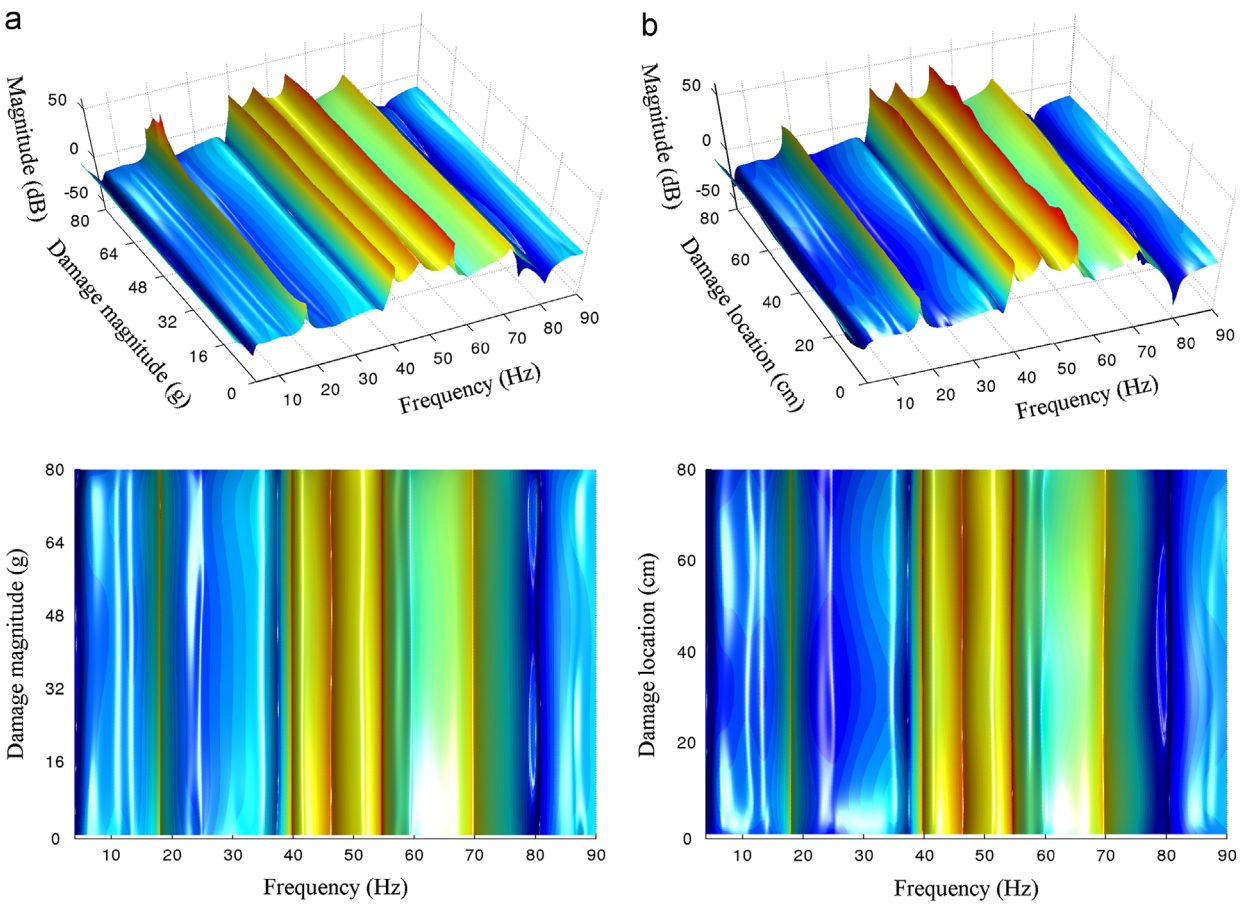

Fig. 4. Damage topology A model ($\mathcal{M}_{k}^{AY}$) based FRF magnitude versus frequency and (a) damage magnitude (for set location $k^2 = 0$ cm) and (b) damage location (for set magnitude $k^1 = 48.792$ g).

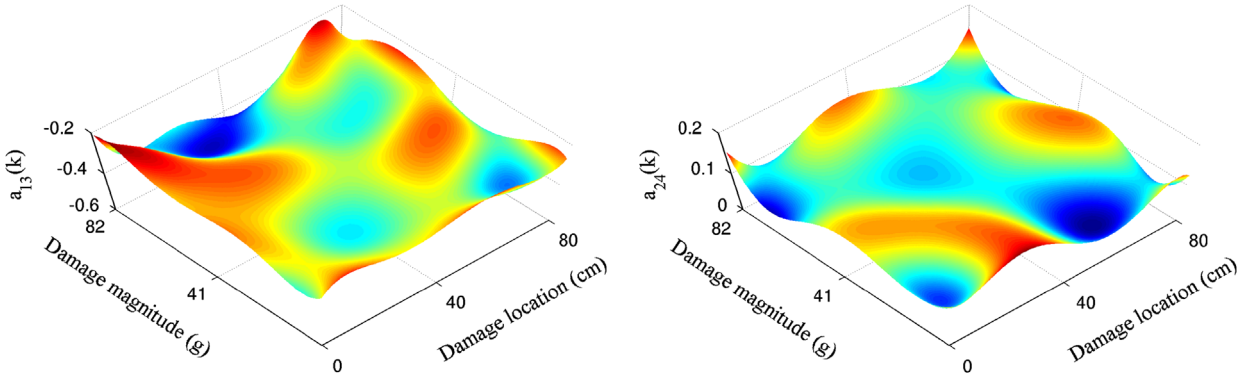

Fig. 5. Typical damage topology A model ($\mathcal{M}_{k}^{AY}$) AR parameters versus damage magnitude (k^1 g) and location (k^2 cm).

once using the Point Y sensor and once using the Point Z sensor. In this way each damage may be either "local" or "remote" depending on the sensor used, so that the capability of the method to operate under either one of the two circumstances is assessed. The ninth Test Case (IX) in Table 4 is "unmodeled", meaning that it does not belong to any one of the three (A, B, C) topologies. Still, it is particularly interesting to examine whether or not its presence can be detected, and whether or not it can be "negatively" localized, the latter meaning whether it can be actually concluded that it does not belong to any of the three considered topologies. An additional question is whether this can be achieved using any one of the three different topology (A or B or C) models; for this reason Test Case IX is considered three times (using both sensors) and the results are designated as IXa, IXb, IXc, respectively.

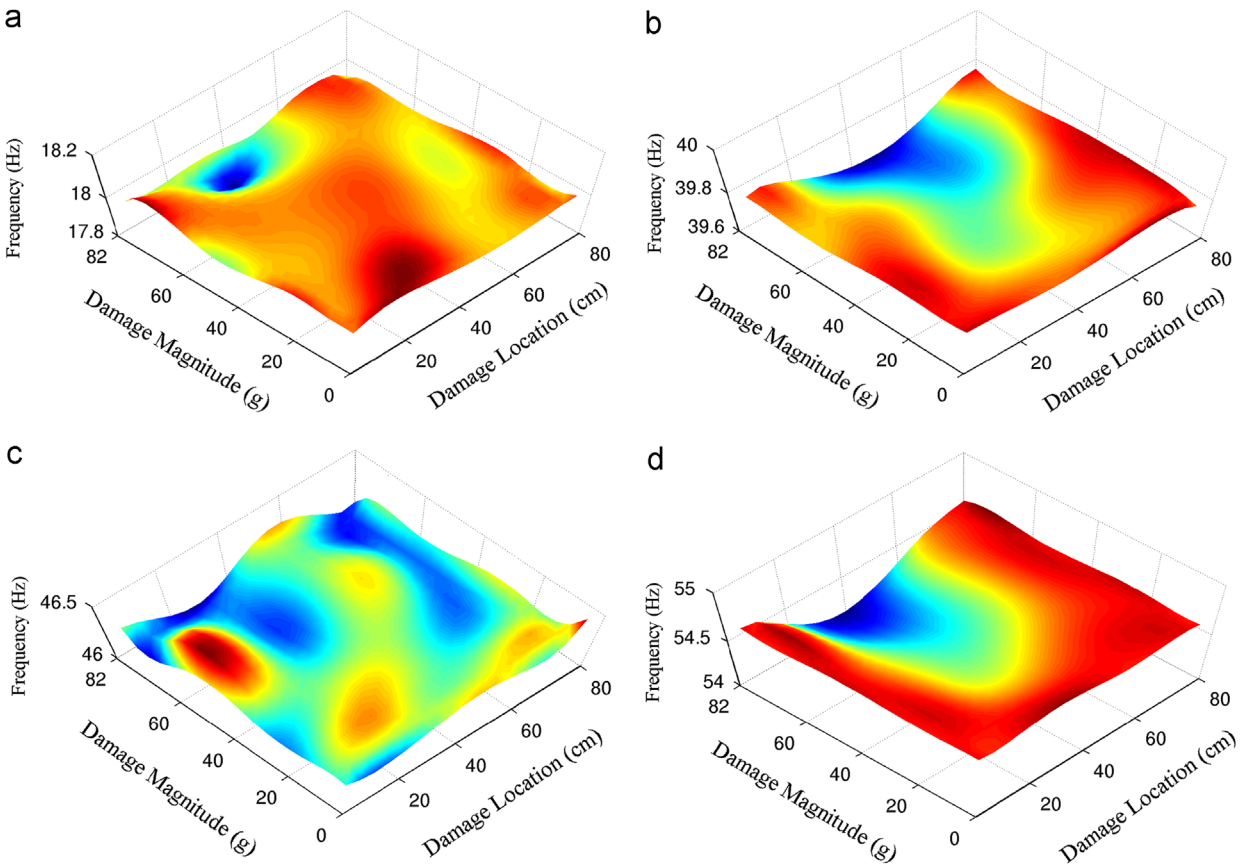

Fig. 6. Indicative natural frequencies versus damage magnitude (k^1 g) and damage location (k^2 cm) based on the damage topology A ($\mathcal{M}_k^{AY}$) model: (a) second mode; (b) third mode; (c) fourth mode; and (d) fifth mode (compare with Table 5 and Fig. 4).

Table 5
Global modal characteristics (natural frequencies and damping ratios) of the structure based on the identified ARX(48, 48) model of the healthy structure.

Structural mode	Natural frequency (Hz)	Damping ratio (%)
1	06.21	8.70
2	17.95	0.33
3	39.80	0.26
4	46.11	0.75
5	54.51	0.04
6	55.37	0.24
8	59.60	3.29
9	69.74	0.78
10	80.11	0.14

Damage detection results for each Test Case and each one of the two response sensors are presented in Fig. 7. Evidently, damage is in all cases clearly detected as the t statistic is where it should be, that is within the dashed lines in the healthy Test Case (I) and beyond them in all damaged Test Cases (II–IXc). Notice that the color code in the bars indicates the actual topology of each considered damage. An important observation here is that all damages are detected, including the "unmodeled" damage, and this is irrespectively of the damage being "local" or "remote" to the sensor used. The importance of this result is related to the fact that even one (or a few, depending on the structure) sensor is sufficient for detecting damage, even if that is taking place at a "remote" location.

Damage topology (mode) identification results for each Test Case are pictorially presented in Fig. 8 separately for each one of the two response sensors. The hypotheses of the current damage belonging to topology A, topology B, or topology C are considered in each Test Case (plot) using the corresponding topology VFP-ARX model. One of these hypotheses is accepted if the corresponding Q statistic is lower than the critical point (dashed horizontal line). The actual damage and its

Table 6
The structure of the identified damage topology models.

Damage topology (mode)	Vibration measurement at Point Y	Vibration measurement at Point Z
A	$\mathcal{M}_{\boldsymbol{k}}^{AY}$: VFP−ARX(48,48)$_{30}$	$\mathcal{M}_{\boldsymbol{k}}^{AZ}$: VFP−ARX(51,51)$_{30}$
B	$\mathcal{M}_{\boldsymbol{k}}^{BY}$: VFP−ARX(57,57)$_{30}$	$\mathcal{M}_{\boldsymbol{k}}^{BZ}$: VFP−ARX(69,69)$_{30}$
C	$\mathcal{M}_{\boldsymbol{k}}^{CY}$: VFP−ARX(44,44)$_{30}$	$\mathcal{M}_{\boldsymbol{k}}^{CZ}$: VFP−ARX(65,65)$_{30}$
Weighted least squares (WLS) estimation		
99 training experiments for damage topology A; 55 training experiments each for topologies B and C		
Frequency range [4–90] Hz, Sampling frequency f_s=256 Hz		
Signal length N=1500 samples (5.85 s)		

Table 7
Genetic algorithm (GA) details for functional subspace dimensionality estimation.

Population size	Elite count	Crossover fraction	Maximum number of generations
100	20	0.7	1000

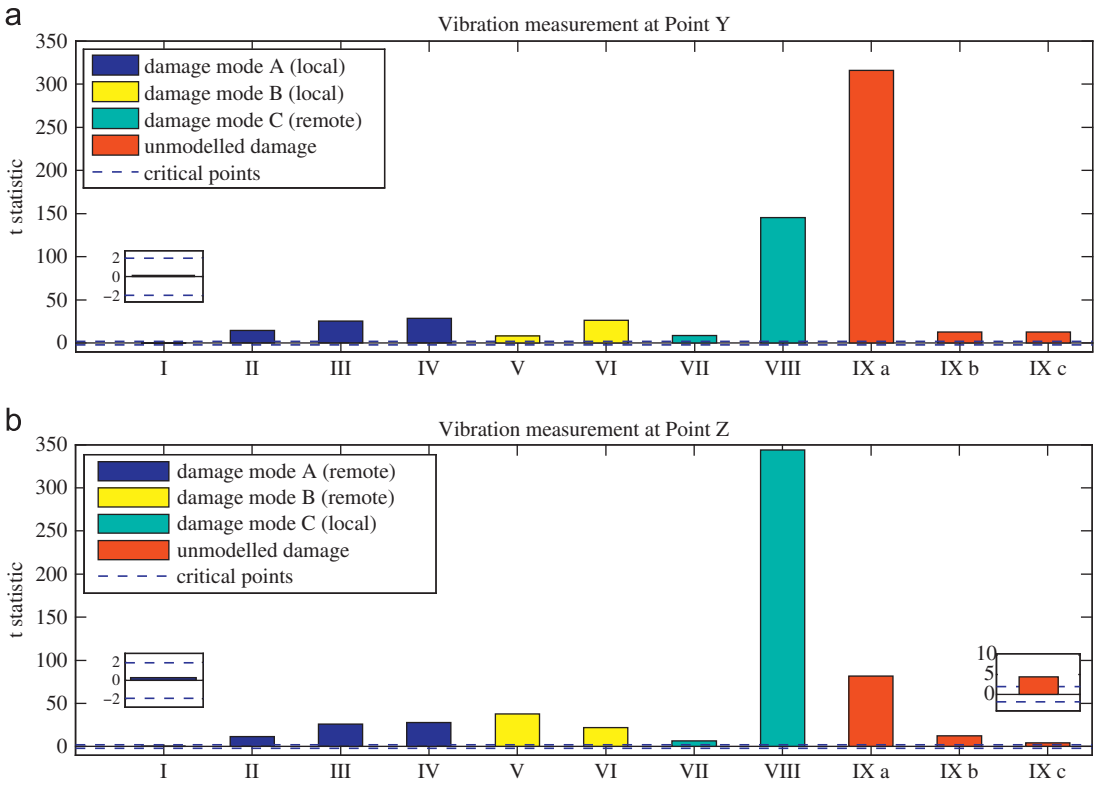

Fig. 7. Damage detection results for the various Test Cases and each vibration measurement position (upper plot: Point Y; lower plot: Point Z): t statistic (bars) and the critical points (- - -) at the $\alpha = 0.05$ risk level. In each Test Case damage is detected if t exceeds the critical point. (For interpretation of the references to color in this figure caption, the reader is referred to the web version of this article.)

characterization as either "local" or "remote" are indicated above each plot. The results of all Test Cases are remarkable, as the actual damage topology (mode) is correctly identified by each one of the two sensors. In the last two plots it is demonstrated that the "unmodeled" damage of Test Case IX is correctly rejected as being associated with one of the A, B, C topologies. These results demonstrate that correct damage topology identification is feasible based on any one of the two sensors, while the same is true for "negative" topology identification of the "unmodeled" damage.

Damage localization and magnitude interval estimation results are presented in Fig. 9 for each Test Case and each one of the two response sensors (both shown in the same plot). It should be noticed that damage detection may be also re-confirmed based on these results, by simply examining whether or not the interval estimate of damage magnitude

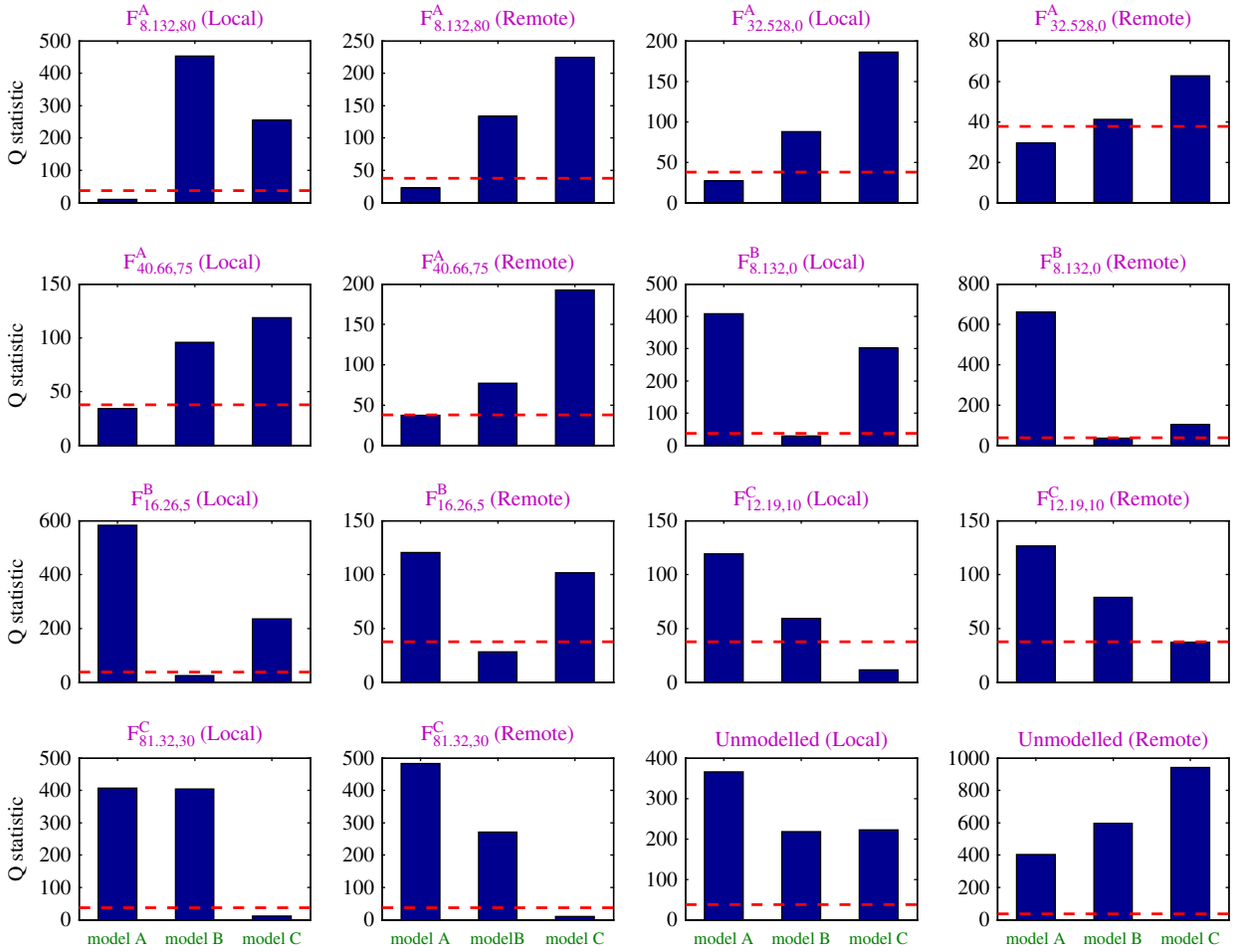

Fig. 8. Damage topology identification results for various Test Cases and each vibration measurement position (Points Y and Z—to be read in rows): in each plot the Q statistic (bar) for the hypothesis of the current damage belonging to each one of the A, B, C topologies is shown relative to the critical point (- - -) at the $\alpha = 0.05$ risk level. A hypothesis is accepted – and the corresponding damage topology is accepted as true – if the Q statistic lies below the critical point. The actual damage and its characterization as "local" or "remote" are indicated above each plot.

(at a certain risk level) includes the zero (no damage)—this is essentially equivalent to the test of Step I of the method. In Test Case I the structure is in fact healthy (F_o), hence the interval estimate of only the damage magnitude is depicted. Evidently, no damage is detected as the interval estimate at the $\alpha = 0.05$ risk level (shaded strip) includes the $k^1 = 0$ value (notice that the dashed vertical line designates the true damage magnitude while the middle line the point estimate and the left and right vertical lines the lower and upper confidence bounds, respectively). In the rest of the Test Cases the bivariate (k^1,k^2) estimates are presented both as point estimates (diamonds) and interval (uncertainty) estimates (ellipsoids) at the $\alpha = 0.05$ risk level. The results obtained by the "local" response sensor are shown as dark (blue), while those obtained by the "remote" sensor as light (magenta). A damage is, in each of these cases, correctly detected as the damage magnitude's interval (uncertainty) estimate does not include the $k^1 = 0$ value (vertical axis). It should be further observed that impressively accurate estimates of the damage magnitude and location, also characterized by narrow uncertainties, are obtained. It is also observed that, in general, the "local" sensors achieve slightly better performance; yet the results are very impressive for all Test Cases.

6. Concluding remarks

A vibration based statistical time series method that is capable of effective damage detection, precise localization, and magnitude estimation within a unified stochastic framework has been introduced. The method is based on the novel extended class of vector-dependent functionally pooled (VFP) models and proper statistical decision making schemes. VFP models are capable of accurately representing a structure in a damaged state for that state's continuum of damage magnitudes and locations on a particular topology. In its inspection phase, the method operates in three distinct steps

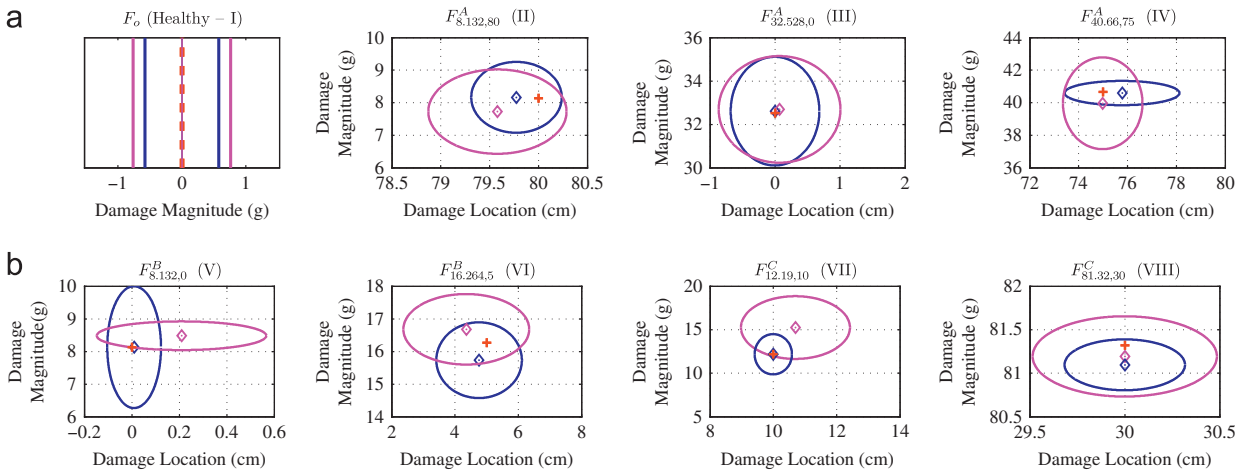

Fig. 9. Damage localization and magnitude interval estimation results: in each plot results of a Test Case in terms of estimated damage magnitude and precise location are presented for two vibration measurement positions (Points Y and Z), one characterized as "local" damage (dark-blue) and the other as "remote" (light-magenta). Damage magnitude and location point estimates are indicated by diamonds and interval (uncertainty) estimates by ellipsoids at the $\alpha = 0.05$ risk level. Damage detection may be also re-confirmed by examining whether the damage magnitude uncertainty includes the zero (no damage) point. In each Test Case the actual damage is indicated by a cross in the diagram as well as above each plot. (For interpretation of the references to color in this figure caption, the reader is referred to the web version of this article.)

taking place within a unified framework: step I involves damage detection, step II involves damage topology identification, and step III involves precise damage localization and magnitude estimation within the identified topology. Damage topologies are continuous, involving an infinite number of potential damage locations; they are presently confined to a single dimensionality but, of course, this may be properly generalized.

The method allows, for the first time within the context of statistical time series and related methods, for complete and precise damage localization on any continuous topology on a structure using a very limited – depending on the size and complexity of the structure – number of sensors. As demonstrated, for "simple" and "limited" size structures even a single pair of excitation–response sensors may be sufficient. Furthermore, estimator uncertainties are fully taken into account in all diagnostic phases, while uncertainty ellipsoids are provided for the damage location and magnitude.

The validity and effectiveness of the method have been experimentally assessed via a proof-of-concept application involving damage detection, precise localization, and magnitude estimation on a prototype GARTEUR-type laboratory aircraft skeleton structure. Damages of different magnitudes occurring on various topologies on the structure (and involving an infinite number of locations within each topology) have been represented by small added masses simulating local stiffness reductions. Although the added masses have been quite small compared to the overall skeleton mass, with their effects on the dynamics being rather minor, the method has proved remarkably effective in detecting damage, identifying the correct damage topology, and then precisely localizing and accurately estimating the damage magnitude. No false alarm or missed damage events have been reported, while the corresponding uncertainty ellipsoids have been impressively accurate, while providing the user with a good feeling about estimation uncertainty.

The main *lessons learnt* and *conclusions drawn* from this study may be summarized as follows:

(i) First and foremost, the study – including the proof-of-concept application – has demonstrated the important fact that effective damage detection, damage topology identification, and damage precise localization and magnitude estimation are possible based on *partial models* of the structural dynamics and a *very limited number of sensors* (even in a single excitation–response signal pair). This is in sharp contrast to methods requiring detailed and "complete" models (such as FEMs) and a multitude of sensors.

(ii) From a slightly different perspective, the study has demonstrated the very significant *amount of information* on the state of the structure embedded even in a single excitation–response signal pair. Thus, an important message is that it may not be necessary to employ a "high" number of sensors for precise damage diagnosis; instead, a "few" sensors and powerful signal analysis for extracting the embedded information may be a much more practical and effective approach.

(iii) The diagnostic performance in terms of damage detection, topology identification, and precise localization and magnitude estimation achieved in the proof-of-concept study (though under controlled laboratory conditions) has been impressive. Damage localization and magnitude estimation are not only excellent at the nominal (point estimation) level, but also at a probabilistic level that provides very accurate and tight uncertainty bounds (ellipsoids).

(iv) A practically important observation is that the diagnosis performance characteristics do *not* appear significantly dependent on the *proximity* of the damage location to the sensor used. Although the uncertainty bounds have been somewhat tighter when estimated by "local", rather than "remote", sensors, this effect has been remarkably limited.

(v) "*Unmodeled*" *damages*, that is damages *not* belonging to any of the considered structural topologies (and thus not modeled in the baseline phase) have been very successfully detected and "negatively" identified as not belonging to the modeled topologies. This is very important as it provides detection and some localization information even for damages for which the method has not been trained.

(vi) The fact that effective damage diagnosis is possible *without* the need for specifically designed excitations and special testing procedures is also very important. Combined with the use of often naturally occurring random excitation and the fact that good results may be obtained with even low/limited frequency bandwidth (4–90 Hz, which includes 10 of the structural modes in the present study) allows for potentially *in-operation* damage diagnosis. The potential use of higher frequency range/bandwidth is expected to lead to further gains in performance.

(vii) The method may operate on *any type* (acceleration, velocity, displacement) of vibration signals and may be modified to be applied to the *output-only case*, where only vibration response signal(s) is(are) available. Naturally, the difficulty is higher in this case, and performance is expected to be affected. This is an issue to be considered in future studies.

(viii) The *price* to be paid for the aforementioned benefits mainly involves the *baseline* (training) phase, and more specifically the identification of the necessary VFP models—yet, this takes place only once, while the inspection phase is simple and automated. Nevertheless, user expertise is necessary in the baseline phase, along with the availability of excitation–response signal records. Although the former is expected to be reduced in the future via more automated procedures, excitation–response signal records still need to be obtained possibly through scale laboratory models or via finite element models (FEMs). Even then, the advantages over alternative (including FEM based) methods remain, in that the FEM is only needed in the baseline phase for inferring the partial and much more "compact" VFP models, and in that no model updating is required in the inspection phase.

(ix) Naturally, a number of issues remain open for future work. Among them are the treatment of multiple damage scenarios (the present method should have no problem with detection, but precise localization or magnitude estimation are not generally possible under the current formulation), as well as operation under varying operating conditions and large uncertainties.

Appendix A. Bivariate polynomials

Bivariate (two-dimensional) orthogonal polynomials may be obtained as *tensor products* from their corresponding (Chebyshev, Legendre, Jacobi, or other [44,53,54]) univariate counterparts. For example, the bivariate Chebyshev orthogonal polynomials have the following form:

$$P_{mn}(x,y) = P_m(x) \cdot P_n(y) \quad (x,y) \in [-1,1] \times [-1,1] \subset \mathbb{R}^2 \tag{A.1}$$

with P_{mn} the bivariate Chebyshev polynomial of total degree mn and $P_m(x)$,$P_n(y)$ the univariate Chebyshev polynomials of degrees m,n, respectively.

Theorem (construction of bivariate polynomial orthogonal basis) [54,53]. *A polynomial orthogonal basis of maximum degree mn contains a total of* $\frac{1}{2}(mn+1)(mn+2)$ *basis functions obtained as follows*:

1. *constant basis function* $P_{0,0}$
2. *linear basis functions* $P_{1,0}$,$P_{0,1}$
3. *quadratic basis functions* $P_{2,0}$,$P_{1,1}$,$P_{0,2}$ □

$\vdots$

$mn+1$. *degree mn basis functions* $P_{mn,0}$,$P_{mn-1,1}$,$P_{mn-2,2}$, …,$P_{1,mn-1}$,$P_{0,mn}$.

The univariate polynomials used in this study in order to obtain their bivariate counterparts are the shifted Chebyshev polynomials of the second kind (Type II Chebyshev polynomials), which belong to the broader family of Chebyshev orthogonal polynomials. These polynomials obey the following recurrence relation:

$$a_{1,n}G_{n+1}(x) = (a_{2,n}+a_{3,n}x)G_n(x) - a_{4,n}G_{n-1}(x) \quad x \in [0,1] \subset \mathbb{R} \tag{A.2}$$

with $a_{1,n} = a_{4,n} = 1$, $a_{2,n} = -2$, $a_{3,n} = 4$, and $G_0(x) = 0$, $G_1(x) = 1$.

Hence, the first five shifted Chebyshev polynomials of the second kind are:

$$P_0 = 1$$
$$P_1 = -1+2x$$
$$P_2 = 1-8x+8x^2$$
$$P_3 = -1+18x-48x^2+32x^3$$
$$P_4 = 1-32x+160x^2-256x^3+128x^4$$

In the present framework, where the two variables are damage magnitude (k^1) and damage location (k^2), the following variable selections are made:

$$x \in [0,1] \subset \mathbb{R},\ x = k^1/k^1_{max} \quad y \in [0,1] \subset \mathbb{R},\ y = k^2/k^2_{max} \tag{A.3}$$

Appendix B. The Bayesian information criterion for VFP-ARX models

Let $\mathcal{M}(\boldsymbol{\theta})$ be a general VFP-ARX model describing a given pool of N sample-long excitation–response signals $z^N = (x^N_{\boldsymbol{k}}, y^N_{\boldsymbol{k}})$. Structure estimation for $\mathcal{M}(\boldsymbol{\theta})$ may then be based on minimization of the Bayesian information criterion (BIC) [33,55]:

$$\widehat{\mathcal{M}}(\widehat{\boldsymbol{\theta}}) = \arg\min_{\mathcal{M}(\boldsymbol{\theta})} \text{BIC}, \quad \text{BIC} = \frac{1}{NM_1M_2}\left\{-L(\boldsymbol{\theta}/z^N) + \dim(\boldsymbol{\theta}) \cdot \frac{\ln(NM_1M_2)}{2}\right\} \tag{B.1}$$

with $L(\cdot)$ designating the natural logarithm of the conditional likelihood of the indicated quantity. The Gaussian log-likelihood function of a VFP-ARX model $\mathcal{M}(\boldsymbol{\theta})$ given the signal samples z^N may be shown to be

$$L(\boldsymbol{\theta}/z^N) = -\frac{NM_1M_2}{2}(\ln 2\pi + 1) - \frac{N}{2}\ln\det\{\boldsymbol{\Gamma}_{\boldsymbol{e}[t]}\} \tag{B.2}$$

Hence, structure estimation for a VFP-ARX model $\mathcal{M}(\boldsymbol{\theta})$ based on BIC minimization may be obtained as

$$\widehat{\mathcal{M}}(\widehat{\boldsymbol{\theta}}) = \arg\min_{\mathcal{M}(\boldsymbol{\theta})} \frac{1}{NM_1M_2}\left\{\frac{N}{2}\ln\det\{\boldsymbol{\Gamma}_{\boldsymbol{e}[t]}\} + \dim(\boldsymbol{\theta}) \cdot \frac{\ln(NM_1M_2)}{2}\right\} = \arg\min_{\mathcal{M}(\boldsymbol{\theta})}\left\{\ln\det\{\boldsymbol{\Gamma}_{\boldsymbol{e}[t]}\} + \dim(\boldsymbol{\theta}) \cdot \frac{\ln(NM_1M_2)}{N_1}\right\}. \tag{B.3}$$

References

[1] S.W. Doebling, C.R. Farrar, M.B. Prime, D.W. Shevitz, Damage identification and health monitoring of structural and mechanical systems from changes in their vibration characteristics: a literature review, Technical Report LA-13070-MS, Los Alamos National Laboratory, 1996.
[2] S.W. Doebling, C.R. Farrar, M.B. Prime, A summary review of vibration-based damage identification methods, Shock Vib. Dig. 30 (2) (1998) 91–105.
[3] C.R. Farrar, S.W. Doebling, D.A. Nix, Vibration-based structural damage identification, R. Soc. Philos. Trans. Math. Phys. Eng. Sci. 359 (2001) 131–149.
[4] D. Montalvão, N.M.M. Maia, A.M.R. Ribeiro, A review of vibration-based structural health monitoring with special emphasis on composite materials, Shock Vib. Dig. 38 (4) (2006) 295–324.
[5] S.D. Fassois, J.S. Sakellariou, Time series methods for fault detection and identification in vibrating structures, R. Soc. Philos. Trans. Math. Phys. Eng. Sci. 365 (2007) 411–448.
[6] S.D. Fassois, J.S. Sakellariou, Statistical time series methods for structural health monitoring, in: C. Boller, F.K. Chang, Y. Fujino (Eds.), Encyclopedia of Structural Health Monitoring, John Wiley and Sons Ltd., 2009, pp. 443–472.
[7] W. Fan, P. Qiao, Vibration-based damage identification methods: a review and comparative study, Struct. Health Monit. 10 (1) (2011) 83–111.
[8] D.C. Zimmerman, H.M. Kim, T.J. Bartkowicz, M. Kaouk, Damage detection using expanded dynamic residuals, J. Dyn. Syst. Meas. Control 123 (2001) 699–705.
[9] A. Nauerz, C.P. Fritzen, Model based damage identification using output spectral densities, J. Dyn. Syst. Meas. Control 123 (2001) 691–698.
[10] Y. Xia, H. Hao, J.M.W. Brownjohn, P.Q. Xia, Damage identification of structures with uncertain frequency and mode shape data, Earthquake Eng. Struct. Dyn. 31 (5) (2002) 1053–1066.
[11] S. Liberatore, G.P. Carman, Power spectral density analysis for damage identification and location, J. Sound Vib. 274 (3–5) (2004) 761–776.
[12] R. Perera, A. Ruiz, C. Manzano, An evolutionary multiobjective framework for structural damage localization and quantification, Eng. Struct. 29 (10) (2007) 2540–2550.
[13] X.G. Hua, Y.Q. Ni, Z.Q. Chen, J.M. Ko, An improved perturbation method for stochastic finite element model updating, Int. J. Numer. Methods Eng. 73 (13) (2008) 1845–1864.
[14] C.R. Farrar, D.A. Jauregui, Comparative study of damage identification algorithms applied to a bridge: I. Experiment, Smart Mater. Struct. 7 (1998) 704–719.
[15] C.R. Farrar, D.A. Jauregui, Comparative study of damage identification algorithms applied to a bridge: II. Numerical study, Smart Mater. Struct. 7 (1998) 720–731.
[16] F.P. Kopsaftopoulos, S.D. Fassois, Vibration based health monitoring for a lightweight truss structure: experimental assessment of several statistical time series methods, Mech. Syst. Signal Process. 24 (2010) 1977–1997.
[17] O.S. Salawu, Detection of structural damage through changes in frequency: a review, Eng. Struct. 19 (9) (1997) 718–772.
[18] M. Basseville, L. Mevel, M. Goursat, Statistical model-based damage detection and localization: subspace-based residuals and damage-to-noise sensitivity ratios, J. Sound Vib. 275 (2004) 769–794.
[19] E.P. Carden, J.M. Brownjohn, ARMA modelled time-series classification for structural health monitoring of civil infrastructure, Mech. Syst. Signal Process. 22 (2) (2008) 295–314.
[20] K.K. Nair, A.S. Kiremidjian, Time series based structural damage detection algorithm using Gaussian mixtures modeling, J. Dyn. Syst. Meas. Control 129 (2007) 285–293.
[21] D.D. Rizos, S.D. Fassois, Z.P. Marioli-Riga, A.N. Karanika, Vibration-based skin damage statistical detection and restoration assessment in a stiffened aircraft panel, Mech. Syst. Signal Process. 22 (2) (2008) 315–337.
[22] Q.W. Zhang, Statistical damage identification for bridges using ambient vibration data, Comput. Struct. 85 (2007) 476–485.
[23] H. Zheng, A. Mita, Two-stage damage diagnosis based on the distance between ARMA models and pre-whitening filters, Smart Mater. Struct. 16 (2007) 1829–1836.
[24] H. Sohn, C. Farrar, N. Hunter, K. Worden, Structural health monitoring using statistical pattern recognition techniques, J. Dyn. Syst. Meas. Control 123 (4) (2001) 706–711.
[25] S.G. Mattson, S.M. Pandit, Damage detection and localization based on outlying residuals, Smart Mater. Struct. 15 (2006) 1801–1810.
[26] G. Manson, K. Worden, D. Allman, Experimental validation of a structural health monitoring methodology: part III. Damage location on an aircraft wing, J. Sound Vib. 259 (2) (2003) 365–385.
[27] J.W. Lee, G.R. Kirikera, I. Kang, M.J. Schulz, V.N. Shanov, Structural health monitoring using continuous sensors and neural network analysis, Smart Mater. Struct. 15 (2006) 1266–1274.

[28] F. Xi, Q. Sun, G. Krishnappa, Bearing diagnostics based on pattern recognition of statistical parameters, J. Vib. Control 6 (2000) 375–392.
[29] U. Jung, B.H. Koh, Structural damage localization using wavelet-based silhouette statistics, J. Sound Vib. 321 (2009) 590–604.
[30] J.S. Sakellariou, S.D. Fassois, Vibration based fault detection and identification in an aircraft skeleton structure via a stochastic functional model based method, Mech. Syst. Signal Process. 22 (2008) 557–573.
[31] J.S. Sakellariou, K.A. Petsounis, S.D. Fassois, On-board fault detection and identification in railway vehicle suspensions via a functional model based method, in: Proceedings of International Conference on Noise and Vibration Engineering, Leuven, Belgium, 2002.
[32] F.P. Kopsaftopoulos, S.D. Fassois, Identification of stochastic systems under multiple operating conditions: the vector dependent FP-ARX parametrization, in: Proceedings of 14th Mediterranean Conference on Control and Automation, Ancona, Italy, 2006.
[33] J.S. Sakellariou, S.D. Fassois, A functional pooling framework for the identification of systems under multiple operating conditions, in: Proceedings of 15th Mediterranean Conference on Control and Automation, Athens, Greece, 2007.
[34] M. Degener, M. Hermes, Ground vibration test and finite element analysis of the GARTEUR SM-AG19 testbed, Technical Report IB 232-96 J 08, Deutsche Forschungsanstalt für Aerolastic, Göttingen, 1996.
[35] E. Balmes, J.R. Wright, Garteur group on ground vibration testing—results from the test of a single structure by 12 laboratories in Europe, in: Proceedings of ASME Design Engineering Technical Conferences, Sacramento, USA, 1997.
[36] F.P. Kopsaftopoulos, S.D. Fassois, Vibration-based structural damage detection and precise assessment via stochastic functionally pooled models, Key Eng. Mater. 347 (2007) 127–132.
[37] E. Papatheou, G. Manson, R. Barthorpe, K. Worden, The use of pseudo-faults for novelty detection in SHM, J. Sound Vib. 329 (2010) 2349–2366.
[38] J.L. Zepico-Valle, M. Garcia-Diegez, M.P. Gonzalez-Martinez, K. Worden, Experimental validation of a new statistical process control feature for damage detection, Mech. Syst. Signal Process. 25 (2011) 2513–2525.
[39] A. Panopoulou,T. Loutas, D. Roulias, S. Fransen, V. Kostopoulos, Dynamic fiber Bragg gratings based health monitoring system of composite aerospace structures, Acta Astron. 69 (7–8) (2011) 445–457. 〈http://dx.doi.org/10.1016/j.actaastro〉. (accesed 2011.05.027).
[40] L. Ljung, System Identification: Theory for the User, second ed. Prentice-Hall, 1999.
[41] T. Söderström, P. Stoica, System Identification, Prentice-Hall, 1989.
[42] S.D. Fassois, Parametric identification of vibrating structures, in: S. Braun, D. Ewins, S. Rao (Eds.), Encyclopedia of Vibration, Academic Press, 2001, pp. 673–685.
[43] J.D. Hios, S.D. Fassois, Stochastic identification of temperature effects on the dynamics of a smart composite beam: assessment of multi-model and global model approaches, Smart Mater. Struct. 18 (2009) 035011. (15pp.).
[44] C. Dunkl, Y. Xu, Orthogonal Polynomials in Several Variables, Cambridge University Press, 2001.
[45] D. Bernstein, Matrix Mathematics, Princeton University Press, 2005.
[46] W.H. Greene, Econometric in Analysis, fifth ed. Prentice-Hall, 2003.
[47] Matlab Global Optimization Toolbox: User's Guide, 2012.
[48] P.E. Gill, W. Murray, M.H. Wright, Practical Optimization, London Academic Press, 1981.
[49] Matlab Optimization Toolbox: User's Guide, 2012.
[50] G.E.P. Box, G.M. Jenkins, G.C. Reinsel, Time Series Analysis: Forecasting & Control, third ed. Prentice Hall, Englewood Cliffs, NJ, 1994.
[51] F.P. Kopsaftopoulos, S.D. Fassois, Scalar and vector time series method for vibration based damage diagnosis in a scale aircraft skeleton structure, J. Theor. Appl. Mech. 49 (3) (2011) 727–756.
[52] F.P. Kopsaftopoulos, S.D. Fassois, Statistical time series methods for damage diagnosis in a scale aircraft skeleton structure: loosened bolts damage scenarios, in: Journal of Physics: Conference Series, Proceedings of the 9th International Conference on Damage Assessment on Structures (DAMAS), vol. 305, Oxford, UK, 2011.
[53] H.L. Krall, I.M. Scheffer, Orthogonal polynomials in two variables, Ann. Mat. Pura Appl. 76 (4) (1967) 325–376.
[54] M.A. Kowalski, The recursion formulas for orthogonal polynomials in n variables, SIAM J. Math. Anal. 13 (2) (1982) 309–315.
[55] G. Schwarz, Estimating the dimension of a model, Ann. Stat. 6 (1978) 461–464.